

Robot-assisted Breast Ultrasound Scanning Using Geometrical Analysis of the Seroma and Image Segmentation

Mojtaba Akbari¹, Jay Carriere¹, Ron Sloboda², Tyler Meyer³, Nawaid Usmani², Siraj Husain³, Mahdi Tavakoli¹

Abstract—In this paper, we propose a robotic ultrasound imaging method that scans the breast in two separate phases to acquire high-quality ultrasound images. Our proposed system controls five Degrees of Freedom (DoFs) of the robot that hold an ultrasound probe to perform precise scanning. This system finds the desired trajectory based on geometrical analysis of the target inside the breast in a pre-scan phase and uses this information to control the probe in a post-scan phase. The proposed method updates the desired values of rotational and translational movement of the probe in the post-scan by calculating the center of mass of segmented target in each acquired frame and the average of image confidence map. The proposed method has been tested experimentally on a plastisol phantom. Given a specific trajectory, the position and orientation of the probe have been controlled at each point of the trajectory. The experiments' result shows us that our proposed visual servoing algorithm successfully controls the probe to look at target tissue and is fast enough for use in a robotic control loop.

I. INTRODUCTION

Ultrasound (US) is a widely used modality in medical imaging. Despite the low signal-to-noise ratio in US images, it is a safe and low-cost medical imaging modality compared to other modalities like Magnetic Resonance Imaging (MRI), Computed Tomography (CT), and X-ray. The quality of the captured US images is related to multiple factors such as intrinsic properties of the US machine, the orientation of the US probe with respect to the tissue surface during scanning, and the contact force between tissue and the probe. While the intrinsic properties of the US machine cannot be changed, the other factors affecting US image quality can be addressed during scanning by using a robotic system holding the US probe.

This research was supported by the Canada Foundation for Innovation (CFI), the Natural Sciences and Engineering Research Council (NSERC) of Canada, the Canadian Institutes of Health Research (CIHR), and the Alberta Jobs, Economy and Innovation Ministry's Major Initiatives Fund to the Center for Autonomous Systems in Strengthening Future Communities.

¹ Mojtaba Akbari, Jay Carriere and Mahdi Tavakoli (Corresponding Author) are with the Department of Electrical and Computer Engineering, University of Alberta, AB, Canada T6G 1H9. akbari@ualberta.ca, jtcarrie@ualberta.ca, mahdi.tavakoli@ualberta.ca

² Ron Sloboda and Nawaid Usmani are with the Department of Oncology, Cross Cancer Institute, 11560 University Avenue, Edmonton, AB, Canada, T6G 1Z2. nawaid.usmani@albertahealthservices.ca, ron.sloboda@albertahealthservices.ca

³ Tyler Meyer and Siraj Husain are with the Division of Radiation Oncology, Tom Baker Cancer Centre, 331 29th Street NW, Calgary, Alberta T2N 4N2. tyler.meyer@albertahealthservices.ca, siraj.husain@albertahealthservices.ca

In hand-held US scanning, the quality of US images depends on the expertise of the sonographer. Robot-assisted US scanning, where the robot holds the US probe, has gained much attention recently [1] as the robotic system can be controlled to automatically generate high-quality images. A robotic US assistant system can work collaboratively with the sonographer, in a semi-autonomous fashion, or fully autonomously. In semi-autonomous robot-assisted US, the system tries to help the sonographer during scanning using haptic feedback or controlling some Degrees of Freedom (DoFs) of the US probe. In fully-autonomous robotic US scanning, the robot controls all positions and orientations of the probe during scanning based on information like acquired image quality, probe-tissue contact force data, or a predefined trajectory. A US scanning robot is usually equipped with force sensors to ensure the force applied to the tissue does not exceed a certain value during scanning. Our proposed method lies in the second category due to the desired repeatability of US scanning. Within this paper, we will propose a fully-autonomous US image scanning algorithm.

Breast cancer is the most commonly diagnosed cancer among women aged 30 to 39 [2]. Commonly available breast cancer treatment options are mastectomy, where the breast is removed, and lumpectomy, where the tumor and a portion of the adjacent tissue are removed. Lumpectomy is followed by external beam radiation therapy to ensure that residual cancer cells are treated. The second method, i.e, breast conservation surgery, is more popular due to cosmetic reasons [3]. Following lumpectomy, the area previously occupied by the tumor is filled with a pocket of bodily fluid called a seroma. An alternative to external beam radiation therapy, which needs many sessions, is permanent seed breast brachytherapy that can be done in one or two sessions. The challenge in breast brachytherapy is to deposit seeds in and around the seroma using needle insertion. The seroma needs to be segmented for accurate needle insertion during radiation therapy. This paper proposes a method to control the probe to keep the seroma in the series of US images acquired during scanning.

In this paper, we propose a visual servoing algorithm that controls five DoFs of the probe during scanning of the breast. The proposed method has two phases called pre-scan and post-scan to analyze the geometrical features of the seroma and design the controller to keep the seroma in the field of view. During the pre-scan phase, we manually segment the seroma inside of the breast US images by moving the probe on the surface of the breast for extracting geometrical

features of it. While in post-scan that may be done on a repeatable basis, we calculate the desired position and orientation of the probe to control the force and steer the probe for better visualization of the seroma based on the acquired US image. This research is motivated by using an autonomous system to have a repeated US post-scan for further required steps like a 3D reconstruction of the breast. The setup is shown in Figure 1.

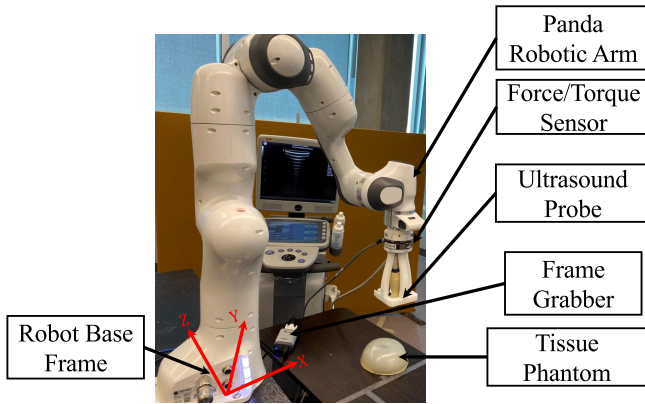


Fig. 1: Robotic US scanning assistant including Panda robot arm, US probe, tissue phantom, frame grabber

The outline of the paper is as follows. In Section II, we will give a brief review of previous robot-assisted sonography and visual servoing algorithms. We develop our proposed US scanning trajectory planning algorithm in Section III that uses pre-scan images for defining 5-DoF trajectory. We will propose our US visual servoing algorithm in post-scan in Section IV, which discusses the specific image features used to control both the position and orientation by updating the trajectory calculated in Section III of the probe during scanning. The experimental setup and results are presented in Section V. Concluding remarks and discussions will be provided in Section VI.

II. BACKGROUND

Robots have shown utility in assisting a sonographer during US scanning. Authors in [4] develop a 4-DoF robotic wrist to perform liver and kidney US imaging. The robotically-held US probe is placed on the patient's body and a sonographer teleoperates the wrist to obtain US images with the robot controller maintaining US scanning force on the patient's body. The authors in [5] propose a cooperative robotic US system to reduce the force that sonographers need to apply during scanning. This system consists of a 6-DoF robotic arm holding the US probe and a dual force sensor setup that enables cooperative control and adaptive force assistance using admittance force control. Authors in [6] develop an impedance-controlled teleoperation system for robot-assisted tele-echography of moving organs such as the heart, chest, and breast that compensates for organ motions. This system implements two impedance models for the local and remote robots with the remote robot following the local robot's trajectory but complying with the oscillatory

interaction-force of moving organs. Authors in [7] propose a solution for energy injected in tele-echography by the operator on the local site based on properly scaling the energy exchanged between the local and the remote site. The authors in [8] give a review of different methods proposed in robot-assisted US intervention and [9] provides a review of the mechanical consideration in designing the robot-assisted US scanning. The methods mentioned in this paragraph are using two robots as a local and remote robots to perform scanning. Using two robots imposes an additional cost to the system and also has a lot of challenges like communication delay or haptic feedback needed in the local robot for the sonographer. This motivates us to propose an autonomous system to perform scanning without using local and remote robots.

Visual servoing information can be gathered from the original US image or a transformed image using wavelet, FFT, or other types of transformations. The challenging part in the implementation of US visual servoing is determining how to relate the position, velocity, and/or force control of the US probe to feature seen in the US image. The method proposed in [10] uses the shearlet transform [11] where the time variation of shearlet decomposition coefficients are linked to the US probe's velocity during scanning. The controller for the robot is based on the error between the current and desired values of the shearlet transformation of the US image. In a similar manner, [12] also uses shearlet transform to control three DoFs of the robot during scanning the x and y direction and angular velocity of the US probe. Authors of [13] propose a method that controls six DoFs of the robot during scanning using the wavelet transformation. The convolution of the acquired US image and wavelet filters is used as a feature vector for controlling the robot during scanning. In addition to wavelet and shearlet transforms, Discrete Cosine Transform (DCT) and Principal Component Analysis (PCA) have also been used for visual servoing. The method proposed in [14] calculates the DCT transformation of the US image and defines the error as a difference between current DCT coefficients and the desired ones. Authors in [14] propose an analytical method for calculating an interaction matrix based on the low-frequency component of DCT coefficients. The author in [15] proposes a visual servoing based on the projection of US image into its orthogonal basis using PCA algorithm. This method evaluates visual servoing performance for both reconstructed images from PCA basis and the basis itself. The method proposed in [16] segments an US frame using a graph-cut strategy and controls in-plane and out-of-plane movement of the probe during scanning by extracting appropriate features from the segmented area and the projection of segmented area on three planes. The method controls 6-DoFs of the robot during scanning.

Confidence map is one of the common preprocessing methods on US images that can be utilized for US image-based visual servoing. The confidence map was proposed in [17] and creates a map based on the attenuation of the US signal inside of the tissue. The author in [18] incorporates the confidence map idea for needle tracking in US images

during needle insertion. The method proposed in [19] uses a confidence map to acquire appropriate features from US images to control three DoFs of the US scanning robot and investigates the relationship between probe positioning and US image quality. The method proposed in [1] uses preoperative MRI images to design a trajectory for the robot for US scanning of the tissue and refines 2-DoFs of this predefined trajectory using features coming from a confidence map. The authors in [20] propose a method based on an image confidence map to track a specific target inside of the tissue during scanning. Here, the controller moves and orients the robot to have a clear view of the target in the acquired US image. Visual servoing algorithms may need to segment the area and acquire image features from the segmented area instead of the whole US image. As we mentioned in this paragraph, the pre-scan data in controlling the US probe are mainly MRI and CT. This motivates us to propose a method that is completely US-based. Using US images in both pre-scan and post-scan reduces the cost of the system and also is a safe option compared to CT and MRI.

The contributions of the paper are as follows. The first novelty of our proposed method is using US image in both phases that is advantageous over previous methods like the method proposed in [1] that uses MRI in the pre-scan phase. The second novelty of our proposed method is proposing a new set of features in designing the trajectory and controlling the orientation and steering the probe during the post-scan phase that considers the visibility of the region of interest without imposing additional computational costs on the system in comparison with [16]. The third novelty of this system is to guarantee the visibility of the seroma in acquired US frames and the contact between the breast and the probe during scanning. This results in a series of high-quality US images acquired by using the proposed method.

III. ULTRASOUND SCANNING TRAJECTORY PLANNING

As previously mentioned, many factors need to be considered during US image acquisition to maintain the quality of the US image. Our proposed method consists of two phases, pre-scan to extract the initial trajectory and post-scan to refine the initial trajectory. The proposed system will extract necessary information from the breast and seroma during the pre-scan, including the location of the seroma inside the tissue. Our US image visual servoing algorithm will then control the US probe's orientation and position during the post-scan phase, utilizing the localized seroma from the pre-scan. The post-scan phase trajectory will be initially designed from this pre-scan information and real-time image processing and visual servoing will be used to refine the orientation and position of the probe throughout the post-scan.

A. Pre-scan Phase

In the pre-scan phase, the probe will be moved on the surface of the breast with an initial position and orientation trajectory either manually, by the sonographer, or through

some naive autonomous US scan. The US image acquired at each point, and the position and orientation of the probe as determined from the robot encoders at each point will be saved for further processing. Within each of the pre-scan US images, the contour of the seroma (region of interest) will be manually segmented. The manually segmented regions within the US images will be used to estimate the location and the shape of the seroma to design the post-scan trajectory. The seroma inside the breast will be approximated as an ellipsoid with frame $\{E\}$ that is defined along the principal axes of the ellipsoid. The dimensions of the ellipsoid are calculated using the manually segmented areas in the US pre-scan image set and principal component analysis. Before US scanning, calibration is done to determine the scale between pixel distances in the US images and real-world distances (in meters).

We will define various coordinate frames shown in Figure 2. These frames are defined to track the movement of the probe during post-scan and relate this movement to each other for estimating the location and shape of the seroma for post-scan. We are going to find the ellipsoid frame $\{E\}$ in space from the pre-scan images centered at the center of the ellipsoid approximated from these images and aligned with principal axes of the ellipsoid. We define intersecting frame $\{C\}$ to calculate the desired value of out-of-plane rotation in this frame that would simplify the calculation. We also introduce US image frame as $\{U\}$ for each pixels value in the image and US probe frame (desired frame) $\{D\}$ to relate the movement of the US probe with respect to other frames attached to the system and acquired features from US image in our proposed control scheme. We can then estimate the dimension of the seroma by a transformation of each point belonging to the segmented region in a pre-scan image to the base frame, i.e., transforming from $\{U\}$ to the $\{B\}$. The mathematical details in calculating frame transformation from $\{E\}$ and $\{U\}$ to $\{B\}$ are ${}^B P = {}^B U T U P$, ${}^B P = {}^B E T E P$. Transformation matrix from $\{B\}$ to $\{D\}$, which is important for our control system is shown as

$${}^D_B T = \left(\begin{array}{c|c} R(\alpha, \beta, \gamma) & \begin{matrix} {}^D P_{x_0} \\ {}^D P_{y_0} \\ {}^D P_{z_0} \end{matrix} \\ \hline 0 \ 0 \ 0 & 1 \end{array} \right), \quad (1)$$

where $[{}^D P_{x_0}, {}^D P_{y_0}, {}^D P_{z_0}]$ is the position of the origin of $\{B\}$ in $\{D\}$.

In Figure 2, we have shown the position and orientation of the probe during the pre-scan phase.

B. Post-scan Phase

The geometrical information of the ellipsoid calculated in the pre-scan phase is being used for calculating the desired values of in-plane, out-of-plane, and $x - y - z$ position of the probe. We are using an axial plane for taking images, which is perpendicular to the trajectory. Hence, we define the orientation of the probe in this plane as in-plane rotation

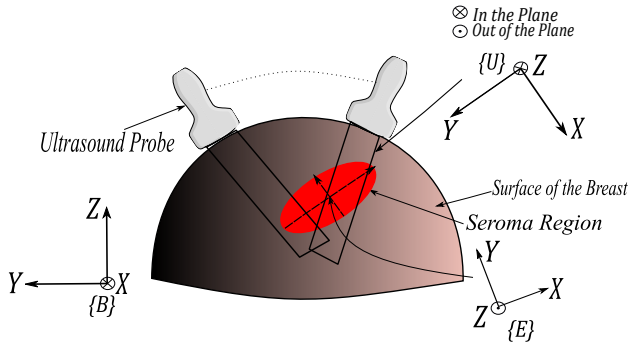


Fig. 2: Visualization of frames attached to the system in pre-scan phase

and the orientation of the probe out of this plane as out-of-plane rotation. We update the in-plane rotation and the movement of the probe in the z direction of the $\{B\}$, as shown in Figures 2 and 3, by segmenting the seroma and using an image confidence map.

1) *Designing Trajectory for Post-scan:* We calculate the desired $x - y - z$ trajectory of the probe on the surface of the breast based on the intersection of a plane containing the principal axis of the ellipsoid (i.e. aligned with the principal axis ${}^E x$ of the seroma) and oriented with the orientation of the this principal axis to have maximum alignment with surface normal of the breast surface. The post-scan trajectory will then be a curve on the surface of the breast resulting from this intersection. We can define our trajectory points as ${}^B P_j = [{}^B x_j, {}^B y_j, {}^B z_j, \alpha_j, \beta_j, \gamma_j]$, which creates a set of point $\Pi = \{{}^B P_j | j = 1, \dots, n\}$. γ or the roll angle of the probe is the part of the trajectory that does not affect our scanning method, hence we are not considering it in our control scheme. The beginning and endpoint of the trajectory are defined as ${}^B P_0$ and ${}^B P_n$, respectively, and are chosen manually on the intersecting curve. The visualization of the frame attached to the system and acquired trajectory is shown in Figure 3.

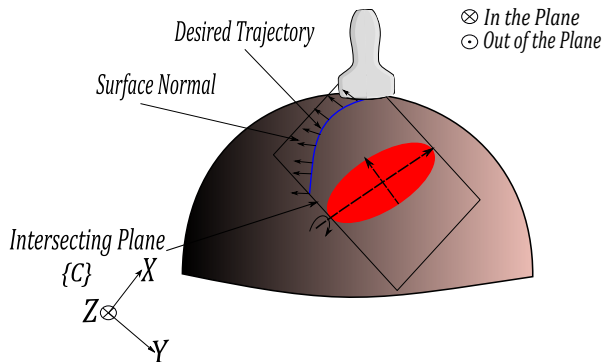


Fig. 3: Designing Trajectory for post-scan phase

The geometrical dimensions of the ellipsoid, containing the seroma, inside the breast are shown in an axial view in Figure 4a and a sagittal view in Figure 4b. Here, the view is defined as a projection of the in two planes from the user view. The desired out-of-plane α_j and in-plane β_j rotations

for points j on the trajectory will be found using geometrical analysis based on the ellipsoid and the surface of the breast.

2) *Finding Desired Out-of-plane Orientation:* The intersecting plane frame $\{C\}$, containing the principal axis of the ellipsoid, allows for finding α_j . The desired out-of-plane rotations are designed to sweep the US probe smoothly as it is translated along the trajectory so that the US probe is always pointed towards a target point ${}^C P_o$. The point ${}^C P_o$ is the point that the line passing through the center of ellipsoid from the surface of the breast intersect with two separate tangents originated from beginning and end point of the trajectory. The visualization of the points coordinates that need to be defined for calculating α_j are shown in Figure 4a. We define the coordinates of the following points in $\{C\}$ using ${}^C T = {}^B T^{-1}$ as ${}^C P_o = {}^C T {}^B P_o$, ${}^C P_n = {}^C T {}^B P_n$, ${}^C P_s = {}^C T {}^B P_s$ and ${}^C P_j = {}^C T {}^B P_j$.

The desired value of out-of-plane rotation α_j can be found in

$$\alpha_j = \text{atan2}({}^C z_s - {}^C z_o, {}^C y_s - {}^C y_o) - \text{atan2}({}^C z_j - {}^C z_o, {}^C y_j - {}^C y_o) \quad (2)$$

between ${}^C P_j$, ${}^C P_s$ and ${}^C P_o$.

3) *Finding Desired In-plane Orientation:* With the out-of-plane orientation α_j of the US probe trajectory defined, we can find the desired value for the in-plane orientation β_j . This process is shown in a sagittal view of the breast in Figure 4b. Here, we are using the center of ellipsoid ${}^B P_m$ which was also found from the pre-scan images.

We define ${}^B P_s$, ${}^B P_j$, and ${}^B P_m$ in the robot base frame $\{B\}$ to calculate desired in-plane orientation. We need to consider surface normal vectors of the breast when finding the desired value of β_j so that the probe is kept in a natural orientation, with respect to the surface of the breast, during scanning. This is shown in

$$\beta_j = \max_i \vec{\beta}_i \cdot \vec{n}_i \quad (3)$$

subject to $i = 1, \dots, \theta$.

that finds the angle which maximizes the dot product between the normal vector and the candidate vectors ($\vec{\beta}$) in a feasible range $(1, \dots, \theta)$. The feasible range can be found by considering the dimension of the probe and the region of interest in each point of the trajectory found in III-B.1. The surface normal vector ${}^B \vec{n}_j$ of the breast in position ${}^B P_j$ within the scanning trajectory is

$${}^B \vec{n}_j = \begin{bmatrix} \frac{\partial f({}^B x_j, {}^B y_j)}{\partial x} \\ \frac{\partial f({}^B x_j, {}^B y_j)}{\partial y} \\ -1 \end{bmatrix}, \quad (4)$$

Which considers the points on the surface of the breast follows the 3D equation as

$${}^B z_j = f({}^B x_j, {}^B y_j). \quad (5)$$

IV. ULTRASOUND VISUAL SERVOING

From Section III, we have developed a 5-DoF trajectory on the surface of the breast for the robot US scanning assistant to

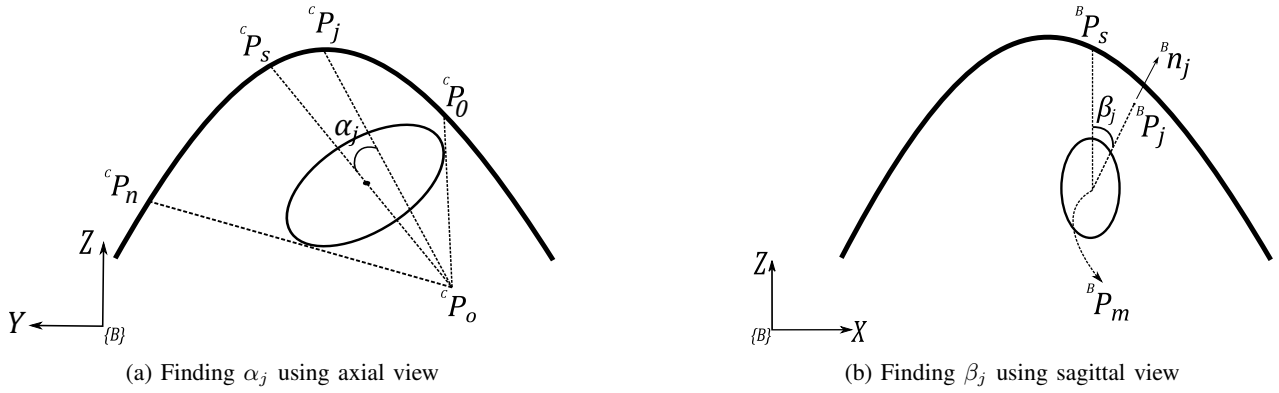


Fig. 4: Finding α_j and β_j using axial and sagittal view

follow. The five DoFs are the $x-y-z$ position of the probe, and the in-plane and out-of-plane rotation of the probe on the surface of the breast. Using visual servoing techniques, we now refine the in-plane angle β_j of the probe and the downward pressure applied to tissue (by modulating ${}^D z_j$) according to information from the US image confidence map and the segmentation of seroma in the US frame.

US images have a low signal-to-noise ratio and need preprocessing to enhance their quality to be used for control purposes. The US confidence map is a commonly used preprocessing method. The US confidence map is a per-pixel measure calculating the probability of a random walk [21] starting from each pixel to reach a number of virtual transducer elements, under specific US constraints [17]. This method considers an US image as a graph where nodes represent the pixels with edges interconnecting the nodes. For our implementation of the confidence map, we will consider a 4-connected neighborhood for each pixel node.

The mean value of the confidence map C_{mean_j} can be considered as an image-based measure of the contact between the breast tissue and the US probe. The desired value of the mean of the confidence map is defined as C_{set} . The ${}^D z_j$ position from the previously found trajectory is updated, in real-time, to increase C_{mean_j} to C_{set} to ensure sufficient probe/tissue contact. The mathematical equation for calculating C_{mean_j} is

$$C_{mean_j} = \frac{1}{M \times N} \sum_{(p_x, p_y) \in S} C(p_x, p_y) \quad (6)$$

where S is the area of the US confidence map, M and N are the height and width of S , and $C(p_x, p_y)$ is the confidence value of pixel located in (p_x, p_y) . The error between current and desired value ($e_{c_j} = C_{mean_j} - C_{set}$) is used as an input to the controller for controlling the ${}^D z_j$ about the original ${}^D z_j$ position calculated in Section III.

The center of the mass of the segmented object is a measure that indicates whether the image intensities are well divided over the segmented region or not. We use this feature to refine our predefined in-plane rotation in the scanning. Here, a US image I_j will be segmented for extracting the seroma. The output is a binary image, in which

the background intensities have 0 values and foreground intensities are 1. The center of mass of the segmented image is a measure for rotating the probe toward the seroma during scanning. We calculate the location of the center of mass in the segmented image as

$$\begin{aligned} {}^U \mu_i &= \frac{1}{I_{tb}} \sum_{(i,j) \in I_b} i \times I_b(i, j) \\ {}^U \mu_j &= \frac{1}{I_{tb}} \sum_{(i,j) \in I_b} j \times I_b(i, j). \end{aligned} \quad (7)$$

Here, ${}^U \mu_i$ and ${}^U \mu_j$ are the coordinate of the center of mass in $\{U\}$, I_b is the binary segmented image, and $I_{tb} = \sum_{(i,j) \in S} I_b(i, j)$. Our segmentation algorithm uses Otsu's threshold method to create a binary image and selects the largest connected component as the seroma inside the breast. The values of ${}^U \mu_i$ and ${}^U \mu_j$ can be transferred to $\{D\}$, resulting in ${}^D \mu_x$ and ${}^D \mu_y$ (${}^D \mu_x = {}^D_U T {}^U \mu_i$ and ${}^D \mu_y = {}^D_U T {}^U \mu_j$). The angle between the central image scan line and the line passing through the center of the mass as determined from the center of the scan line defines an error that can be used to control the in-plane rotation of the probe during scanning. The mathematical expression for finding the in-plane rotation error e_{β_j} is

$$\begin{aligned} e_{\beta_j} &= \text{atan2}\left({}^U \mu_j - \frac{M}{2}, {}^U \mu_i\right) - \\ &\quad \text{atan2}\left({}^U \mu_{d,j} - \frac{M}{2}, {}^U \mu_{d,i}\right) \end{aligned} \quad (8)$$

where ${}^U \mu_{d,i}$ and ${}^U \mu_{d,j}$ are the coordinate of desired value. A visual illustration of how the value e_{β_j} is calculated is shown in Figure 5.

A. Ultrasound Scanning Robot Controller

From the trajectory found in Section III and the visual serving information demonstrated in Section IV, we can now describe our control law for the position and orientation of the US probe during the post-scan. This controller considers the position and orientation of the probe in $\{D\}$ as ${}^D P = [{}^D x_p, {}^D y_p, {}^D z_p, {}^D \alpha_p, {}^D \beta_p, {}^D \gamma_p]^t$. The desired value of the robot's position and orientation in $\{D\}$ is denoted as ${}^D P_d = [{}^D x_d, {}^D y_d, {}^D z_d, {}^D \alpha_d, {}^D \beta_d, {}^D \gamma_d]^t$. Here, the initial $x-y-z$

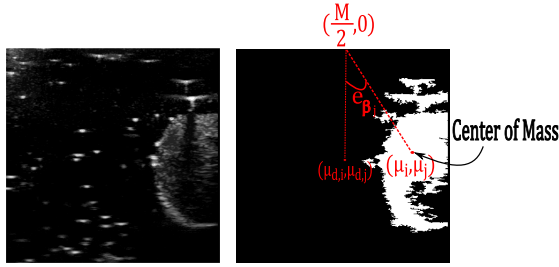


Fig. 5: Center of the mass and calculation of e_{β_j} using segmented US frame

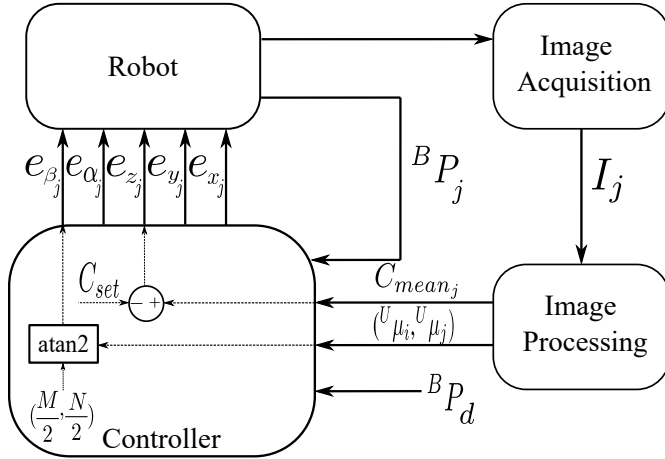


Fig. 6: Control loop of post-scan phase

z position of a trajectory calculated from Section III-B.3. The initial and desired value of in-plane rotation and out-of-plane rotation for any points of the trajectory are β_j and α_j respectively, which were calculated in Section III-B.3 and III-B.2. The desired value of the probe position in the z direction ${}^D z_d$ and in-plane rotation will also be updated using e_{c_j} and e_{β_j} as ${}^D z_d = {}^D z_d + k_1 e_{c_j}$, ${}^D \alpha_d = {}^D \alpha_d + k_2 e_{\beta_j}$. The error between the current point and the desired one is being used for controlling the robot during scanning calculated by

$${}^D P_d = \begin{bmatrix} {}^D x_d \\ {}^D y_d \\ {}^D z_d + k_1 e_{c_j} \\ \alpha_j \\ \beta_j + k_2 e_{\beta_j} \\ {}^D \gamma_d \end{bmatrix}, {}^D E_j = \begin{bmatrix} {}^D x_d - {}^D x_p \\ {}^D y_d - {}^D y_p \\ {}^D z_d + k_1 e_{c_j} - {}^D z_p \\ \alpha_j - {}^D \alpha_p \\ \beta_j + k_2 e_{\beta_j} - {}^D \beta_p \\ {}^D \gamma_d - {}^D \gamma_p \end{bmatrix} \quad (9)$$

Here, k_1 and k_2 are gains assigned to the corresponding features to relate them to the velocity of the robot.

The error ${}^D E_j$ is an input to a PID controller to control both the position and orientation of the probe during scanning. The image acquisition block, which is a US machine, sends an image to the receiver for calculating C_{mean_j} and e_{β_j} by using confidence map mean from (6) and the segmented center of mass from (7). The control loop is shown in Figure 6 and the algorithm is demonstrated in Algorithm 1, where ϵ , δ_1 , and δ_2 are the tolerance of the position and orientation error in the proposed system.

Algorithm 1 Proposed US Scanning Controller

Require: Desired position and orientation of the probe of the probe (${}^D x_d, {}^D y_d, {}^D z_d, {}^D \alpha_d, {}^D \beta_d, {}^D \gamma_d$), ϵ , δ_1 , δ_2

- 1: **while** $e_{c_j} \geq \epsilon$ and $e_{\alpha} \geq \delta$ and $e_{\beta} \geq \delta_2$ **do**
- 2: **if** $e_{c_j} \leq \epsilon$ **then**
- 3: Update the ${}^D z_d$
- 4: $e_{c_j} = C_{mean_j} - C_{set}$
- 5: **end if**
- 6: **if** $e_{\alpha} \geq \delta_1$ and $e_{\beta} \geq \delta_2$ **then**
- 7: Update ${}^D \alpha_d$ using (2)
- 8: $e_{\alpha} = {}^D \alpha_d - \alpha_j$
- 9: Update the ${}^D \beta_j$ using (3) and (8)
- 10: $e_{\beta} = {}^D \beta_j - \beta_j$
- 11: **end if**
- 12: **end while**

V. EXPERIMENT AND RESULTS

In this study, an Axia80-M20 force-torque sensor (ATI Industrial Automation, Apex, NC, USA) is mounted on a Panda robotic arm (Franka Emika GmbH, Munich, Germany) and an adapter was built to hold an US probe (see Figure 1). The US machine used for the experiment was an Ultrasonix Touch with a 4DL14-5/38 Linear 4D transducer (Ultrasonix Corp, Richmond, BC, Canada). For this experiment, we only used the 2D functionality of the US probe. Images from the US machine were captured in real-time with an Epiphan DVI2USB3.0 (Epiphan Systems Inc, California, USA) for processing. For our experiment, we used a tissue phantom made of plastisol.

The controller was programmed and implemented in MATLAB 2019a (The Mathworks Inc, Natwick, MA, USA) and ran using Simulink on a PC running Ubuntu 16.04 LTS. The PC has an Intel Core i5-8400 running at 4.00 GHz. The communication between robot and computer was done over UDP.

The pre-scan phase consisted of moving the US probe on the surface of the phantom tissue and recording the applied forces and US probe positions. The seroma within this initial image set was manually segmented and the parameters, including the principal axis and center, of the approximated seroma ellipsoid, was found. We designed our post-scan trajectory based on the output of the pre-scan phase. During the post-scan phase, the robot moved the probe along the surface of the phantom and the algorithm changed the values of $x - y$ position, α_j , β_j and force applied to the surface of the phantom. The evaluation is based on three main criteria, which are reported in Figure 7 for five different points on the trajectory, with five different desired out-of-plane and in-plane rotations, on the surface of the phantom calculated using (2) and (3). The evaluation metrics are the norm of the error in the probe's orientation with respect to the desired in-plane and out-of-plane rotation as

$$\|e_{\alpha, \beta}\|^2 = \|({}^D \alpha_p - {}^D \alpha_d, {}^D \beta_p - {}^D \beta_d)\|^2, \quad (10)$$

the variation of β_j which results in movement of the center

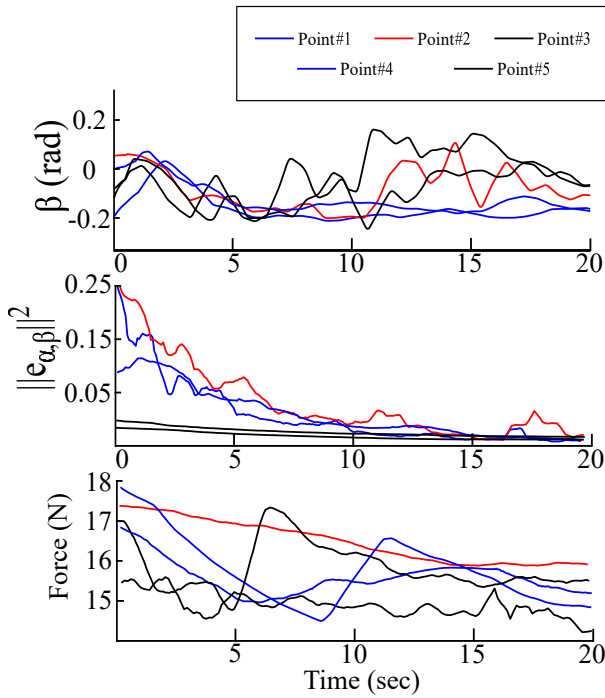


Fig. 7: Experimental results for variation of β , $\|e_{\alpha,\beta}\|^2$ and force

of mass, and the force applied to the phantom during the experiment.

The variation of error norm $\|e_{\alpha,\beta}\|^2$ reported in Figure 7 shows our proposed method is able to decrease the norm of the error in each point of the trajectory. It also indicates that our method works even when there is a change in the in-plane rotation caused by the movement of the center of mass. Figure 7 shows our proposed controller compensates for deviation of the probe orientation caused by the movement of the center of mass, with the probe being reoriented successfully to keep the center of mass on the center of an image frame. This guarantees that our proposed method keeps the seroma in the center of the acquired US image as the variation converges to 0 for each point. The force values reported in the last figure of Figure 7 show that our proposed method applies a reasonable amount of force during scanning. This level of force does not cause deformation for the tissue during scanning. We have also calculated the average of these criteria for the five points within Table I.

TABLE I: Average of $\|e_{\alpha,\beta}\|^2$, deviation of β_j and force values in five separate points on the trajectory

Point	$\ e_{\alpha,\beta}\ ^2$	Deviation of β_j	Force
Point #1	0.04 ± 0.048	-0.19 ± 0.015 (rad)	16.01 ± 0.314 (N)
Point #2	0.07 ± 0.057	-0.06 ± 0.021 (rad)	16.84 ± 0.397 (N)
Point #3	0.01 ± 0.007	0.01 ± 0.021 (rad)	15.31 ± 0.217 (N)
Point #4	0.06 ± 0.022	-0.06 ± 0.016 (rad)	16.14 ± 0.645 (N)
Point #5	0.01 ± 0.006	-0.02 ± 0.019 (rad)	16.20 ± 0.455 (N)

In this paper, we proposed a method to define a 5-DoF US scanning trajectory based on the geometrical features of a target seroma within the breast. A visual servoing algorithm method was used to update two of the controlled DoFs in real-time during scanning to ensure sufficient probe contact and to better visualize the seroma within the US images. Our proposed trajectory generation and visual servoing method, referred to as the post-scan, was based on information captured during a manual pre-scan set of images. The pre-scan images can be captured at arbitrary orientations and positions, with the pose of the US probe was recorded as the pre-scan images are capture. The pre-scan images were processed to extract geometrical information of the seroma inside the breast. The seroma was approximated by an ellipsoid, with the center of the ellipsoid and principal axis being used as part of the geometrical analysis to define the post-scan trajectory. For the post-scan, we calculated the desired US probe trajectory through the intersection of a plane (containing the ellipsoid principal axis) with the surface of the breast. The intersection points on the surface of the breast then form the desired $x - y - z$ trajectory of the US probe. The in-plane and out-of-plane rotation of the probe is calculated at each point of the trajectory via geometrical analysis of the seroma inside of the breast. The in-plane orientation of the probe is updated using an online segmentation algorithm that locates the center of the seroma and orients the probe to point towards it. The desired value of the z position of the probe was also updated, using the average confidence map calculated from the US image during scanning, to ensure sufficient contact between the breast and the probe. The proposed method was evaluated experimentally using plastisol phantoms. The experimental results show that our proposed method orients the probe to keep the seroma in the center of acquired image and keeps the probe in contact with the phantom with minimum deformation.

In the future, we will work on a 3D reconstruction algorithm that is able to generate a 3D volume of the breast using pre-scan images automatically to be able to control the remaining DoF of the robot during visual servoing. This additional information will help the proposed method locate the seroma more precisely for the post-scan phase. The other feature that can be added to the system is to propose a new set of features that is able to control the probe when a needle is inserted inside the breast to have a good visualization of the seroma and needle together during scanning.

REFERENCES

- [1] M. Welleweerd, A. de Groot, S. de Looijer, F. Siepel, and S. Stramigioli, "Automated robotic breast ultrasound acquisition using ultrasound feedback," in *2020 IEEE International Conference on Robotics and Automation (ICRA)*. IEEE, 2020, pp. 9946–9952.
- [2] K. D. Miller, M. Fidler-Benaoudia, T. H. Keegan, H. S. Hipp, A. Jemal, and R. L. Siegel, "Cancer statistics for adolescents and young adults, 2020," *CA: A Cancer Journal for Clinicians*, vol. 70, no. 6, pp. 443–459, 2020.

- [3] E. R. Fisher, J. Wang, J. Bryant, B. Fisher, E. Mamounas, and N. Wolmark, "Pathobiology of preoperative chemotherapy: findings from the national surgical adjuvant breast and bowel project (nsabp) protocol b-18," *Cancer: Interdisciplinary International Journal of the American Cancer Society*, vol. 95, no. 4, pp. 681–695, 2002.
- [4] F. Najafi and N. Sepehri, "A robotic wrist for remote ultrasound imaging," *Mechanism and machine theory*, vol. 46, no. 8, pp. 1153–1170, 2011.
- [5] T.-Y. Fang, H. K. Zhang, R. Finocchi, R. H. Taylor, and E. M. Boctor, "Force-assisted ultrasound imaging system through dual force sensing and admittance robot control," *International journal of computer assisted radiology and surgery*, vol. 12, no. 6, pp. 983–991, 2017.
- [6] M. Sharifi, H. Salarieh, S. Behzadipour, and M. Tavakoli, "Tele-echography of moving organs using an impedance-controlled telerobotic system," *Mechatronics*, vol. 45, pp. 60–70, 2017.
- [7] E. Sartori, C. Tadiello, C. Secchi, and R. Muradore, "Tele-echography using a two-layer teleoperation algorithm with energy scaling," in *2019 International Conference on Robotics and Automation (ICRA)*. IEEE, 2019, pp. 1569–1575.
- [8] M. Antico, F. Sasazawa, L. Wu, A. Jaiprakash, J. Roberts, R. Crawford, A. K. Pandey, and D. Fontanarosa, "Ultrasound guidance in minimally invasive robotic procedures," *Medical image analysis*, vol. 54, pp. 149–167, 2019.
- [9] A. A. Moshahi and F. Najafi, "A review of robotic mechanisms for ultrasound examinations," *Industrial Robot: An International Journal*, 2014.
- [10] L.-A. Duflot, A. Krupa, B. Tamadazte, and N. Andreff, "Towards ultrasound-based visual servoing using shearlet coefficients," in *2016 IEEE International Conference on Robotics and Automation (ICRA)*. IEEE, 2016, pp. 3420–3425.
- [11] G. Easley, D. Labate, and W.-Q. Lim, "Sparse directional image representations using the discrete shearlet transform," *Applied and Computational Harmonic Analysis*, vol. 25, no. 1, pp. 25–46, 2008.
- [12] L.-A. Duflot, A. Krupa, B. Tamadazte, and N. Andreff, "Shearlet-based vs. photometric-based visual servoing for robot-assisted medical applications," in *2016 IEEE/RSJ International Conference on Intelligent Robots and Systems (IROS)*. IEEE, 2016, pp. 4099–4104.
- [13] M. Ourak, B. Tamadazte, O. Lehmann, and N. Andreff, "Direct visual servoing using wavelet coefficients," *IEEE/ASME Transactions on Mechatronics*, vol. 24, no. 3, pp. 1129–1140, 2019.
- [14] E. Marchand, "Direct visual servoing in the frequency domain," *IEEE Robotics and Automation Letters*, vol. 5, no. 2, pp. 620–627, 2020.
- [15] —, "Subspace-based direct visual servoing," *IEEE Robotics and Automation Letters*, vol. 4, no. 3, pp. 2699–2706, 2019.
- [16] C. Nadeau, A. Krupa, J. Petr, and C. Barillot, "Moments-based ultrasound visual servoing: From a mono-to multiplane approach," *IEEE Transactions on Robotics*, vol. 32, no. 6, pp. 1558–1564, 2016.
- [17] A. Karamalis, W. Wein, T. Klein, and N. Navab, "Ultrasound confidence maps using random walks," *Medical image analysis*, vol. 16, no. 6, pp. 1101–1112, 2012.
- [18] M. K. Welleweerd, D. Pantelis, A. G. de Groot, F. J. Siepel, and S. Stramigioli, "Robot-assisted ultrasound-guided biopsy on mr-detected breast lesions," in *2020 IEEE/RSJ International Conference on Intelligent Robots and Systems (IROS)*. IEEE, 2021, pp. 2965–2971.
- [19] P. Chatelain, A. Krupa, and N. Navab, "Optimization of ultrasound image quality via visual servoing," in *2015 IEEE international conference on robotics and automation (ICRA)*. IEEE, 2015, pp. 5997–6002.
- [20] —, "Confidence-driven control of an ultrasound probe: Target-specific acoustic window optimization," in *2016 IEEE International Conference on Robotics and Automation (ICRA)*. IEEE, 2016, pp. 3441–3446.
- [21] L. Grady, "Random walks for image segmentation," *IEEE transactions on pattern analysis and machine intelligence*, vol. 28, no. 11, pp. 1768–1783, 2006.